Acta Crystallographica Section D
Biological Crystallography
ISSN 0907-4449

X-ray and neutron protein crystallographic analysis of the trypsin–BPTI complex

Kenji Kawamura,[a] Taro Yamada,[b] Kazuo Kurihara,[c] Taro Tamada,[c] Ryota Kuroki,[c] Ichiro Tanaka,[b,d] Haruyuki Takahashi[a] and Nobuo Niimura[b]*

[a]Institute of Applied Beam Science, Graduate School of Science and Engineering, Ibaraki University, 4-12-1 Naka-Narusawa, Hitachi, Ibaraki 316-8511, Japan, [b]Frontier Research Center for Applied Atomic Sciences, Ibaraki University, Ibaraki Quantum Beam Research Center, 162-1 Shirakata, Tokai, Ibaraki 319-1195, Japan, [c]Molecular Structural Biology Group, Quantum Beam Science Directorate, Japan Atomic Energy Agency, 2-4 Shirakata-Shirane, Tokai, Ibaraki 319-1195, Japan, and [d]Department of Biomolecular Functional Engineering, The College of Engineering, Ibaraki University, 4-12-1 Naka-Narusawa, Hitachi, Ibaraki 316-8511, Japan

Correspondence e-mail: niimura@mx.ibaraki.ac.jp

Received 10 November 2010
Accepted 20 December 2010

PDB Reference: trypsin–BPTI complex, 3otj.

In this work, the crystal structure of the β-trypsin–bovine pancreatic trypsin inhibitor (BPTI) complex was refined and the D and H atoms in the complex were identified using data from both 1.6 Å resolution X-ray diffraction and 2.15 Å resolution neutron diffraction. After crystallization in an H_2O solution, the sample crystal was soaked in a D_2O solution for about two weeks. The protonation states of the catalytic triad (Asp102, His57 and Ser195) were observed. These results confirmed that the nucleophilic reactivity of the hydroxyl group of Ser195 was increased by forming a hydrogen bond with His57. According to structural analysis, the trypsin–BPTI interfaces located at the scissile peptide and the active sites were inaccessible to solvent water, and the amide H atoms of P2′ Arg17/I, Gly216/E and Gly193/E at the binding interface were protected from H/D exchange. In contrast, both the amide H atom of P1′ Ala16/I of the scissile peptide bond P1–P1′ and the H atom between His57 $N^{\varepsilon 2}$ and Ser195 O^{γ} were replaced by D atoms. The hydrogen-bond networks at the S1 pocket were also confirmed and discussed from the viewpoint of substrate recognition. Moreover, the first neutron crystallographic structure of the Michaelis complex state of trypsin–BPTI is presented.

1. Introduction

Bovine pancreatic trypsin inhibitor (BPTI, Kunitz-type) is one of the most widely studied serine protease inhibitors (Greene *et al.*, 1966; Fritz & Wunderer, 1983; Liu *et al.*, 1971; Laskowski & Sealock, 1971; Wagner & Wüthrich, 1982; Huber *et al.*, 1970; Vincent & Lazdunski, 1972). It has been established that this protein strongly inhibits bovine trypsin (Vincent & Lazdunski, 1972) and interacts with various other serine proteases, including plasmin, kallikrein, factors Xa and XIIa, thrombin, protein C, trypsin and chymotrypsin (Otlewski *et al.*, 2001; Krowarsch *et al.*, 2005). It can also act as a noncovalent protease inhibitor which does not bind covalently to the active site of a target enzyme. Instead, this type of protease inhibitor interferes with proteolytic activity through a tight Michaelis complex (Otlewski *et al.*, 2005). Specifically, it inhibits catalytic activity by forming a bond between the protease and its binding loop with a geometric alignment labelled P3–P3′ (termed a canonical conformation), which is substrate-like (Schechter & Berger, 1967; Bode & Huber, 1992; Otlewski *et al.*, 2005).

The target enzyme of BPTI, bovine trypsin, is a well known serine protease. This protein is a member of the chymotrypsin family of proteases and its active residues are His57, Ser195

and Asp102 (based on the numbering of residues in chymotrypsin). The catalytic mechanism of trypsin has been extensively studied and the reaction mechanism of this protease has been suggested in many previous reports. Trypsin is specific for basic amino acids (lysine and arginine) and the substrate-recognition site is Asp189 (Voet *et al.*, 1999; Hedstrom, 2002; Bode & Huber, 1992).

The first complex structures of BPTI with bovine trypsin were determined by Rühlmann *et al.* (1973) and Huber *et al.* (1974). These studies revealed that the distance between the Ser195 O^{γ} atom and the carbonyl C atom of the P1–P1′ peptide bond of BPTI is 2.6 Å. This interatomic distance is shorter than that of a van der Waals contact, but is insufficient to form a covalently bonded tetrahedral intermediate state (Huber & Bode, 1978; Huber *et al.*, 1974). Laskowski and coworkers have suggested that the inhibition mechanism of noncovalent inhibitors involves the use of a protease inhibitor with the same activity as BPTI, whereby a hydrolysis product is resynthesized by kinetic control. Specifically, the reactive site P1–P1′ forms an acyl enzyme and the acyl bond formed prevents deacylation by the hydrolytic water (Laskowski & Wu, 1953; Finkenstadt & Laskowski, 1967; Ardelt & Laskowski, 1983, 1985; Laskowski & Qasim, 2000). Furthermore, Radisky & Koshland (2002) presumed that the cleaved peptide bond of P1–P1′ is resynthesized by the reverse reaction owing to the presence of a tightly bound leaving amine in the structure of noncovalent inhibitors of serine protease in the complexed state.

Recently, Zakharova *et al.* (2009) provided further insight into the resynthesis of the P1–P1′ peptide bond on the atomic scale by performing high-resolution (1.46 Å) crystal structure analysis of a BPTI*–S195A complex (where BPTI* indicates cleaved BPTI). However, because the protonation states of the active sites in trypsin have not been observed for the catalytic reaction in the trypsin–BPTI complex, the details of this reaction at the atomic level remain unclear. In the present study, we carried out neutron crystal structure analysis of the trypsin–BPTI complex because this type of analysis can reveal the protonation states of the active sites in enzymes (Niimura & Bau, 2008; Blakeley *et al.*, 2008; Blakeley, 2009). Using this approach, we successfully obtained the protonation states of the catalytic triad.

To date, the neutron crystal structures of the trypsin–MIP (1-methylethyl dihydrogen phosphate propan-2-yl dihydrogen phosphate; Kossiakoff, 1984) and elastase–FRW (4-{[(2*S*)-3-methyl-1-oxo-1-((2*S*)-2-{[(3*S*)-1,1,1-trifluoro-4-methyl-2-oxopentan-3-yl]carbamoyl}pyrrolidin-1-yl)butan-2-yl]carbamoyl} benzoic acid; Tamada *et al.*, 2009) complexes have been determined and the protonation states of the histidine in the catalytic triad and the oxyanion hole have been discussed. Unlike BPTI, these inhibitors are irreversible and bind covalently to the hydroxyl O atom of serine in the catalytic group. Of note, the free BPTI structure, which is not in an enzyme–inhibitor complex state, has also been refined using X-ray and neutron data (Wlodawer *et al.*, 1984). Differentiating the protonation states of the trypsin–BPTI complex from those of the above-mentioned complexes would provide a more complete insight into the catalytic process of serine proteases, as well as into the inhibition mechanism of BPTI.

In most neutron experiments, protein solutions are subjected to H_2O/D_2O exchange prior to crystallization or the crystals are soaked in D_2O after crystallization in H_2O solution. These techniques allow D atoms to replace many existing H atoms, not only in the solvent water molecules but also in the protein molecules at sites containing 'exchangeable' H atoms (mostly the H atoms of N—H and O—H bonds exposed to the solvent). Nevertheless, some potentially exchangeable sites resist deuteration and remain hydrogenated. Presumably, some NH groups resist H/D exchange because of their poor solvent accessibility or tight binding owing to strong hydrogen bonds. Protein–ligand interactions and related protein properties have previously been studied by examination of H/D-exchange reactions: specifically, whether or not the H atoms of amides, hydroxyl groups in active sites and functional amino-acid residues are exchanged for D atoms (Cotten *et al.*, 1999; Englander *et al.*, 1996; Garcia *et al.*, 2004; Hamuro *et al.*, 2003; Fasoli *et al.*, 2009). Recent NMR and mass-spectrometric studies have also highlighted the importance of H/D exchange in studies of the dynamic behaviour of proteins (Simon *et al.*, 1984; Wales & Engen, 2006; Kaltashov *et al.*, 2009). By using crystals that had been crystallized in H_2O solution and soaking them in D_2O solution for different durations, we previously discovered that the time evolution of the H/D-exchange ratios of RNase A and T_6 insulin crystals varies from location to location in the folding structures of these proteins. These experiments suggest that the H/D-exchange ratio provides information about the dynamic behaviour of proteins (Iwai *et al.*, 2009; Yagi *et al.*, 2009).

Similarly, neutron crystal structure analysis of the trypsin–BPTI complex has provided significant information about the trypsin–BPTI interaction by revealing the H/D exchange of the H atoms in the amide/hydroxyl groups. In this study, we observed H/D exchange of the amide H atoms at P1′ Ala16 (in the reactive site located in the binding loop of BPTI) despite the fact that these atoms are located in the interior of the complex. This observation may reveal the mechanism by which noncovalent protein inhibitors interact with enzymes.

2. Materials and methods

2.1. Samples

Recombinant bovine β-trypsin (23 300 Da) from corn and BPTI (6511 Da) from bovine pancreas were purchased from Acris Antibodies GmbH and Sigma–Aldrich, respectively. β-Trypsin and BPTI were dissolved in 20 m*M* HEPES buffer pH 7.5 to concentrations of 30.0 and 10.4 mg ml^{-1}, respectively. Thus, the molar ratio of β-trypsin to BPTI was 1:1.25, which was that used in a previous study (Hanson *et al.*, 2007). A suitable crystal was obtained by the sitting-drop vapour-diffusion method. A BD Falcon organ-culture dish with a 60 mm centre well from Becton, Dickinson & Co. was used as the crystallization vessel. An 18 mm siliconized circular cover slide was placed in the centre well. 3 ml reservoir solution,

which consisted of 1.45 *M* ammonium sulfate, 200 m*M* HEPES buffer pH 7.5 and 10 m*M* calcium chloride, was placed into the outer well and the vessel was sealed with silicon vacuum grease. A 200 µl droplet was prepared on the siliconized glass plate in the centre well by mixing equal volumes of reservoir and protein solutions. The crystal used for the neutron study grew to 2.2 mm^3 (2.0 × 1.1 × 1.0 mm) in two weeks at 298 K. In order to reduce background scattering from H nuclei, the crystal grown in the H_2O solution was soaked in deuterated mother liquor at pD 7.9 for two weeks at 298 K. This technique allowed D atoms to occupy 'exchangeable' H sites such as NH and OH groups, especially those exposed to the solvent.

2.2. X-ray and neutron data collection, processing and reduction

The crystal was sealed in a quartz glass tube. The neutron diffraction experiment was carried out at room temperature using the BIX-4 single-crystal diffractometer installed at the 1G beam port of the JRR-3 reactor at the Japan Atomic Energy Agency (JAEA; Kurihara *et al.*, 2004). The wavelength of the neutrons was 2.6 Å. The diffraction data were collected by the step-scan method with an interval of 0.3° and the exposure time was 4 h per frame. The intensities of the reflections were integrated and scaled using the *HKL* suite v.1.97.2 (Otwinowski & Minor, 1997). Data were processed to 2.15 Å resolution.

An X-ray diffraction experiment was performed at room temperature on the BL-6A beamline at the Photon Factory (PF) at KEK in Japan. The reflection data were recorded on a Quantum 4R detector from Area Detector Systems Corporation (ADSC). We used a wavelength of 1.0 Å with an oscillation range of 1.0° and a total rotation angle of 180°. We used the same crystal sample in this experiment as used in the neutron diffraction experiment. The obtained reflection data were treated with the *HKL*-2000 program (Otwinowski & Minor, 1997). X-ray data were processed to 1.6 Å resolution.

The detailed statistics for both the X-ray and neutron data are summarized in Table 1.

Table 1
X-ray and neutron crystallographic data-collection statistics and crystal structure-refinement statistics.

These statistics were calculated using the input file for 'model_stat' in the program *nCNS*. Values in parentheses are for the highest resolution shell.

	Neutron	X-ray
Data collection		
Space group	*I*222	
Unit-cell parameters		
a (Å)	75.78	75.60
b (Å)	85.53	85.36
c (Å)	123.10	122.55
Beam source	JAEA JRR-3	KEK PF BL-6A
Wavelength (Å)	2.6	1.0
Diffractometer	BIX4	ADSC Quantum 4R
Exposure time per frame	4 h	1 s
Total No. of frames	275	180
Observed reflections	48802	377031
Unique reflections	20552	52224
Resolution (Å)	37.89–2.15 (2.23–2.15)	35.94–1.60 (1.64–1.60)
$\langle I/\sigma(I)\rangle$	5.42 (2.22)	27.85 (2.12)
Completeness (%)	92.6 (90.9)	99.3 (100)
R_{merge}†	0.144 (0.363)	0.061 (0.334)
Structure refinement		
Space group	*I*222	
Unit-cell parameters		
a (Å)	75.60	
b (Å)	85.36	
c (Å)	122.55	
Resolution (Å)	37.89–2.15 (2.19–2.15)	35.94–1.60 (1.63–1.60)
R_{work}‡	0.209 (0.304)	0.197 (0.245)
R_{free}‡	0.226 (0.283)	0.209 (0.259)
No. of reflections in working set	19307 (947)	49539 (2461)
No. of reflections in test set	1038 (48)	2630 (103)
No. of reflections used	20345	52169
Luzzati coordinate error (Å)	0.25 [5.0–2.15 Å]	0.19 [5.0–1.60 Å]
No. of water molecules	120	
No. of D atoms	496	
No. of atoms with calculated H/D-exchange ratio	350	
R.m.s.d. bonds (Å)	0.013	
R.m.s.d. angles (°)	1.4	
R.m.s.d. dihedrals (°)	15.6	
R.m.s.d. impropers (°)	21.1	
Average *B* factor (Å^2)	24.3	

† $R_{merge} = \sum_{hkl}\sum_i |I_i(hkl) - \langle I(hkl)\rangle| / \sum_{hkl}\sum_i I_i(hkl)$, where $I_i(hkl)$ is the intensity of the *i*th observation of reflection *hkl* and $\langle I(hkl)\rangle$ is the average intensity. ‡ $R = R_{free} = \sum_{hkl} ||F_{obs}| - |F_{calc}|| / \sum_{hkl} |F_{obs}|$ calculated for the reflections of the working and test sets, respectively. R_{free} was calculated using 5% of the reflections that were randomly selected for cross-validation.

2.3. Structure refinement

X-ray and neutron joint structure refinements were carried out with the program *nCNS*, which is a version of *CNS* modified for the purpose of neutron refinement (Adams *et al.*, 2009; Table 1). Model building in real space was carried out with *Coot* (Emsley & Cowtan, 2004). The crystal structure of the Protein Data Bank (PDB) entry 2ptc (Marquart *et al.*, 1983) was used as an initial model. The H and D atoms were generated with this initial model using the default topology and parameter files for the *nCNS* program (Adams *et al.*, 2009), and all water molecules were stripped. This initial model was further refined with a simulated-annealing step. Subsequently, atom-position minimization, *B*-factor refinement and real-space refinement were executed. At the same time, D_2O molecules were assigned for only the peaks in the difference Fourier nuclear-scattering map; as shown in Table 1, 120 D_2O molecules were assigned. After the overall structure was determined, the H/D-exchange ratio was calculated with occupancy refinement for the amide and hydroxyl H atoms (see §2.4 for details). Since the occupancy factors of H atoms are strongly correlated to their *B* factors, those parameters were refined several times iteratively.

2.4. H/D-exchange calculation

The H/D-exchange ratio was calculated using the strategy provided in the *nCNS* program. This program treats an exchangeable H site as a single D atom with a variable apparent occupancy q_{nCNS}. *nCNS* allows q_{nCNS} to have a value ranging from −0.56 to 1, according to the occupancies of H and D. For example, an H nucleus [with a neutron scattering length (b_H) of -0.375×10^{-12} cm] is expressed as a D nucleus

[with a neutron scattering length (b_D) of 0.667 $\times$ 10^{-12} cm] with a negative occupancy factor of −0.56 (*i.e.* −0.375/0.667). The apparent occupancy factor (q_{nCNS}) gives the normalized occupancy factors for D and H (q_D and q_H) at an exchangeable site from the following equations:

$$q_D = \frac{(b_D \times q_{nCNS} - b_H)}{(b_D - b_H)}$$
$$q_H = 1 - q_D. \quad (1)$$

In the current study, it was assumed that some exchangeable sites have slow H/D-exchange rates and maintain H because of steric hindrance, interaction with nearby atoms or crystal packing. Therefore, q_{nCNS} values were refined for the following three cases: (i) all amide H atoms in main chains, (ii) H atoms in amides or hydroxyl groups in side chains, which bind to N or O atoms with no accessible surface area (ASA), and (iii) H atoms shared with donor and acceptor atom pairs, which have stronger interactions than van der Waals contacts. The ASA for each atom was calculated with *AREAIMOL* within *CCP*4 (Collaborative Computational Project, Number 4, 1994). For other cases, we assumed that H/D exchange occurred quickly and the occupancy factor of D was fixed at 1.0. Finally, the occupancies for 350 out of 496 D atoms were refined.

Coordinates and structure factors have been deposited in the PDB with code 3otj.

3. Results and discussion

3.1. Protonation states of the catalytic triad

The specific roles of His N$^{\varepsilon2}$ within the catalytic triad of serine proteases are as follows: to act as a base and extract the H from the OH group of serine, to act as an acid and transfer H to the scissile peptide amide, to act as a base and extract the H from a hydrolytic H_2O molecule and to act as an acid and transfer H to the deprotonated O^- of the hydroxyl group of serine. The protonation state of His57 N$^{\varepsilon2}$ is crucial to understanding the catalytic mechanism of trypsin because N$^{\varepsilon2}$ serves as both a base and an acid for activating the nucleophilic species of Ser195 and for transferring a proton to the leaving NH group in the substrate polypeptide, respectively. In this study, we used neutron crystal structure analysis to examine the protonation (deuteration) states of the catalytic triad (Asp102, His57 and Ser195) of trypsin in the complexed state with BPTI, which is a Michaelis complex state. Fig. 1 shows the $F_o - F_c$ nuclear scattering map of both His57 D$^{\delta1}$ and Ser195 D$^{\gamma}$ in the trypsin–BPTI complex; this map was made at the 5.5σ contour level and was calculated without incorporation of the D atoms. Using this method, we found two positive peaks: one between Asp102 O$^{\delta2}$ and His57 N$^{\delta1}$ and the other between His57 N$^{\varepsilon2}$ and Ser195 O$^{\gamma}$. The distances between Asp102 O$^{\delta2}$ and D$^{\delta1}$ and between D$^{\delta1}$ and His57 N$^{\delta1}$ were determined to be 2.0 and 1.0 Å, respectively. The distance between Asp102 O$^{\delta2}$ and His57 N$^{\delta1}$ was 2.8 Å and the O$^{\delta2}$—D$^{\delta1}$—N$^{\delta1}$ angle was ∼140°. The distances between His57 N$^{\varepsilon2}$ and D$^{\gamma}$ and between D$^{\gamma}$ and Ser195 O$^{\gamma}$ were determined as 1.3 and 1.7 Å, respectively. The distance between His57 N$^{\varepsilon2}$ and Ser195 O$^{\gamma}$ was 2.8 Å and the N$^{\varepsilon2}$—D$^{\gamma}$—O$^{\gamma}$ angle was ∼144°.

Since the interpretation of the observed protonation states should be carried out in conjunction with X-ray crystallographic analysis, we also used this method to examine the complex of BPTI with trypsin. In the trypsin–BPTI complex there is apparently no covalent bond between Ser195 O$^{\gamma}$ and the carbonyl C atom of the reaction site P1–P1′; no covalent bond has been observed between them in electron-density maps from X-ray diffraction analyses in previous studies (Rühlmann *et al.*, 1973; Huber *et al.*, 1974; Marquart *et al.*, 1983). However, this structure in the X-ray analysis should be interpreted as only one aspect of the catalytic steps that occur in the trypsin–BPTI complex. Another of the catalytic steps involves His57 extracting an H atom from the Ser195 OH group, forming a tetrahedral intermediate structure, and thereby causing the nucleophilic reactivity of the hydroxyl group of serine to increase. However, this nucleophilic attack on Ser195 O$^{\gamma}$ has not been observed using X-rays. This catalytic step does correspond to the protonation states observed by neutron diffraction; that is, in the neutron crystal structure the D atom was observed midway between His57 N$^{\varepsilon2}$ and Ser195 O$^{\gamma}$. This observation is plausible because it is inconceivable that the Ser195 OH group would be deprotonated and yet the negatively charged O would remain stable. Thus, our observation of D$^{\gamma}$ between His57 N$^{\varepsilon2}$ and Ser195 O$^{\gamma}$ in the trypsin–BPTI complex indicates that some interaction exists between D$^{\gamma}$ and Ser195 O$^{\gamma}$. We cannot judge from the current data whether our observation is a consequence of the deuteration effect as emphasized by Fisher & Helliwell (2008).

It is informative to compare our present results with those of previous neutron diffraction analyses of serine protease analogue–inhibitor complexes. Two structures of these com-

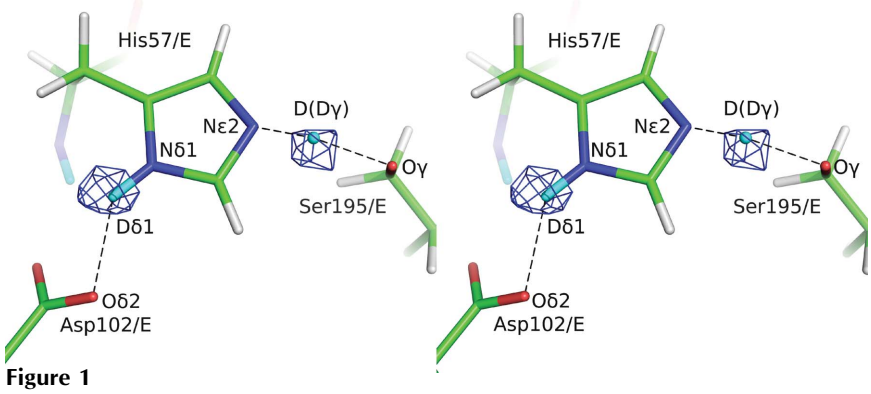

Figure 1
$F_o - F_c$ nuclear scattering map (in stereoview) of the catalytic triad in the trypsin–BPTI complex. The maps were calculated without the D$^{\delta1}$ and D$^{\gamma}$ atoms and are contoured at the 5.5σ density level. Each broken line indicates a hydrogen bond between a D atom and an acceptor atom. This figure was prepared with *PyMOL* (DeLano, 2002).

plexes determined by neutron diffraction experiments have been reported to date. Specifically, these structures are of elastase–FR130180 (PDB entry 3hgn; Tamada *et al.*, 2009) and trypsin–MIP (PDB entry 1ntp; Kossiakoff, 1984) complexes. Both FR130180 and MIP form tetrahedral intermediate structures with the serine proteases. The Ser195 O^{γ} atoms of the serine proteases are chemically bonded to the compounds with a bond length of 1.5 Å. The imidazole ring of histidine extracts the H atom from Ser195 O^{γ} and it is subsequently doubly protonated in both complexes. Other researchers have observed the protonation state of the catalytic triad in the tetrahedral intermediate form, but to our knowledge we are the first to have observed it in the Michaelis complex state. Thus, our observation confirms the previously suggested idea that histidine increases the nucleophilic reactivity of serine by forming a hydrogen bond to it. In addition, this experimental finding implies that the catalytic reaction advances the scission of the peptide bond.

3.2. The network of hydrogen bonds in the S1 pocket domain

The network of hydrogen bonds in the S1 pocket domain, which is the specific binding site of trypsin, has been confirmed by neutron diffraction analysis. The structural parameters of the hydrogen bonds between P1 Lys15/I and S1 Asp189/E in the S1 pocket domain play particularly important roles in the molecular-recognition mechanism of this enzyme (Bode & Huber, 1992).

The S1 pocket is the region at which trypsin recognizes P1 Lys15 of BPTI. The network of hydrogen bonds in the S1 pocket of trypsin provides insight into the stability caused by substrate binding. The detailed structure of this network is depicted as a scheme of arrows in Fig. 2(*a*), in which each arrow indicates the direction from a donor to an acceptor. The related parameters of the network are also summarized in Table 2. Moreover, the $2F_o - F_c$ nuclear scattering map of the domain is shown in Fig. 2(*b*). The protonation states of ε-amine-ND_3^+ of the key residue Lys15/I were clearly observed. We found that the $D^{\zeta1}$ atom of Lys15/I was linked to Ser190/E by bifurcated hydrogen bonds: $D^{\zeta1}\cdots O^{\gamma}$ and $D^{\zeta1}\cdots O$. Moreover, the bond between the $D^{\zeta2}$ atom of Lys15/I and Val227/E was mediated by the hydration H_2O molecule DOD1014/E through hydrogen bonding; the $2F_o - F_c$ nuclear-scattering map of this bond is shown in Fig. 2(*b*). The $D^{\zeta3}$ atom of Lys15/I was hydrogen bonded to Asp189/E through the hydration H_2O molecule DOD1008/E. The H/D exchange ratios of $D^{\zeta1}$ and $D^{\zeta2}$ were both 100% and that of $D^{\zeta3}$ was 78%. The negative charge of the carboxyl group $-COO^-$ of Asp189/E serves to strengthen the interaction through the mediator DOD1008/E. This interaction contributes to the recognition of BPTI by trypsin.

The structure of the network of hydrogen bonds of other atoms is shown in Fig. 2 and the related parameters are summarized in Table 2. These networks seem to contribute to the stability of trypsin–BPTI complex formation.

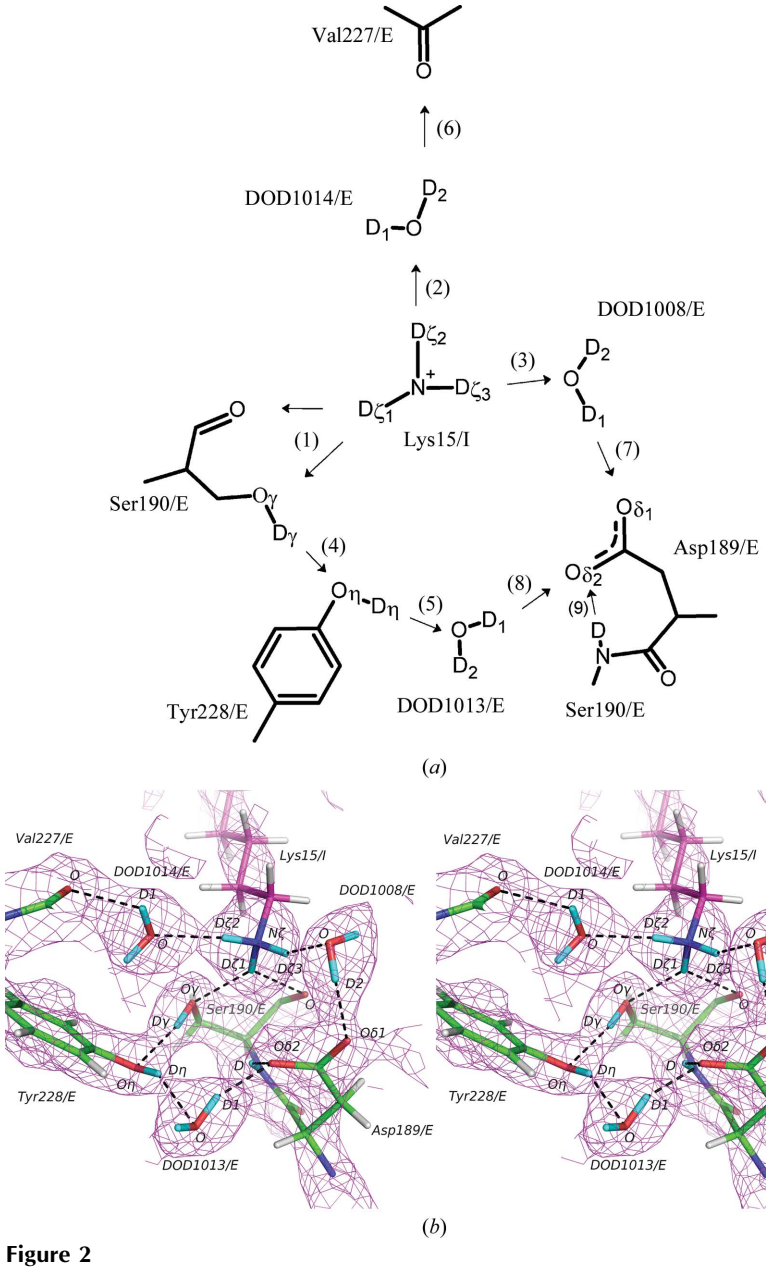

Figure 2
Network of hydrogen bonds in the S1 pocket region. (*a*) A schematic diagram that indicates the directions of the hydrogen bonds from donor H atoms to acceptor atoms. The number in parentheses beside each arrow corresponds to the number used in Table 2. This scheme was prepared with *ChemSketch* (Li *et al.*, 2004). (*b*) $2F_o - F_c$ nuclear scattering maps (in stereoview) of the S1 pocket region contoured at 1.5σ. This figure was prepared with *PyMOL*.

Table 2
H/D-exchange ratio, *B* factor of the donor D atom and hydrogen-bond geometry in the trypsin–BPTI interface and the hydrogen-bond network between the P1 and S1 pocket region.

No.‡	Donor atom	Donor H atom	Acceptor atom	Bond length§ (Å)	Bond length¶ (Å)	Angle†† (°)	ASA by residue† (Å^2) Donor	ASA by residue† (Å^2) Acceptor	D ratio (%)	Donor H *B* factor (Å^2)
Hydrogen bonds in the S1 pocket of trypsin										
1	Lys15/I N$^{\zeta1}$	D$^{\zeta1}$	Ser190/E O$^{\gamma}$	3.03	2.2	136	0	0	97	17.5
	Lys15/I N$^{\zeta1}$	D$^{\zeta1}$	Ser190/E O	2.98	2.3	124				17.5
2	Lys15/I N$^{\zeta1}$	D$^{\zeta2}$	DOD1014/E O	2.92	2.0	146		n/a‡‡	100	15.3
3	Lys15/I N$^{\zeta1}$	D$^{\zeta3}$	DOD1008/E O	2.82	1.9	152			78	15.2
4	Ser190/E O$^{\gamma}$	D$^{\gamma}$	Tyr228/E O$^{\eta}$	2.82	1.9	169	0	1	94	18.6
5	Tyr228/E O$^{\eta}$	D$^{\eta}$	DOD1013/E O	2.62	1.8	137	1	n/a	83	16.0
6	DOD1014/E O	D1	Val227/E O	2.87	2.2	129	n/a	0	n/a	18.1
7	DOD1008/E O	D2	Asp189/E O$^{\delta1}$	2.72	2.0	135		3		17.3
8	DOD1013/E O	D1	Asp189/E O$^{\delta2}$	2.70	1.8	153		3		21.6
9	Ser190/E N	D	Asp189/E O$^{\delta2}$	2.72	1.9	146	0	3	100	18.5
Amide H atoms at the interface between the main chains of trypsin and BPTI										
	Gly216/E N	D	Pro13/I O	3.10	2.3	141	1	15	0	15.6
	Lys15/I N		Ser214/E O	3.20	2.3	128	0	2	24	13.1
	Ser195/E N		Lys15/I O	2.86	1.9	160	0	0	87	14.4
	Gly193/E N		Lys15/I O	2.68	1.8	151	1		6	13.3
	Arg17/I N		Phe41/E O	2.94	2.0	155	40	0	2	13.6
Asn43										
	Asn43/I N$^{\delta2}$	D$^{\delta21}$	Gln7/I O	3.03	2.1	151	5	98	0	14.6
	Asn43/I N$^{\delta2}$	D$^{\delta22}$	Tyr23/I O	3.16	2.2	167		9	7	14.9

† ASA indicates accessible surface area by residue in non-water calculation. ‡ As labelled in Fig. 2. § Distance between the donor and acceptor atoms. ¶ Distance between the donor H atom and the acceptor atom. †† Donor–H–acceptor angle. ‡‡ ASA for DOD was not calculated because of the definition.

3.3. The structure of the trypsin–BPTI interface including the oxyanion hole

We also obtained the H/D-exchange ratios of the amide H atoms at the interface between the main chains of trypsin and BPTI (Table 2). Fig. 3 shows the $F_o - F_c$ nuclear scattering map of this interface, which was calculated without inclusion of H atoms. (The blue and red contours show the $+3.0\sigma$ and -3.0σ levels, respectively.) The amide H atoms of P1 Lys15/I, P2′ Arg17/I, Gly216/E and Gly193/E (this last residue is part of the oxyanion hole) were protected from H/D exchange. These exchange ratios were 24, 2, 0 and 6%, respectively. These data indicate that Arg17/I, Gly193/E, Lys15/I and Gly216/E form strong hydrogen bonds to Phe41/E, Lys15/I, Ser214/E and Pro13/I, respectively. However, the amide H atoms of Ser195 (which is part of the oxyanion hole) were replaced by D atoms, although the calculated ASA values of the region of interest were quite small, as shown in Table 2. The H/D-exchange ratio of the amide H atoms of Ser195 was determined to be 87%. In contrast, the Gly193/E NH group was apparently protected against H/D exchange as the ASA value of the Gly193 was almost zero.

Tamada *et al.* (2009) revealed that an oxyanion hole exists in the elastase–FR130180 complex structure according to neutron crystal structure analysis. The crystal that was used in this study was grown in D_2O solution, such that D atoms replaced the H atoms that formed hydrogen bonds in the oxyanion hole. The two hydrogen bonds that formed the oxyanion hole were considered to be equivalent based on their H/D-exchange ratios. In contrast, in the trypsin–BPTI complex the hydrogen bond between Lys15 O and Gly193 NH was stronger than that between Lys15 O and Ser195 NH and the former bond was protected from the H/D-exchange reaction. Thus, the two hydrogen bonds formed by the acceptor of the carboxyl O of Lys15/I, which forms the oxyanion hole, may not be equivalent. Gly193, which is a component of the oxyanion hole, belongs to one of the trypsin–BPTI binding interfaces.

3.4. Asn43 contributes to the rigidity of BPTI

In the context of a complex, the inhibitory effect of a natural inhibitor is dependent on the flexibility of the target enzyme. It is assumed that the rigidity of BPTI in the trypsin–BPTI complex is caused by several amino acids with high homology that exist in other Kunitz-type serine protease inhibitors, such as the amino acids in the canonical binding loop or those in the three disulfide bridges Cys5–Cys55, Cys14–Cys38 and Cys30–Cys50 (Deisenhofer & Steigemann, 1975; Wlodawer *et al.*, 1984, 1987). Asn43/I is one of the most highly conserved residues in BPTI homologues (Pritchard & Dufton, 1999; Dufton, 1985).

We found that the two H atoms of the NH_2 group in the side chain of Asn43/I were protected against the H/D-exchange reaction, as shown in Fig. 4. The exchange ratios of H$^{\delta21}$ and H$^{\delta22}$ were determined to be 0 and 7%, respectively, although the side chain was located close to the exterior of the molecule. These NH_2 H atoms of the Asn43/I side chain were also found to form hydrogen bonds to the O atoms of Tyr23/I and Glu7/I. The atomic distance Asn43/I D$^{\delta21}\cdots$Glu7/I O was 2.1 Å and the atomic distance Asn43/I D$^{\delta22}\cdots$Tyr23/I O was 2.2 Å. The other detailed structural parameters are given in Table 2.

It is thought that Asn43/I is one of the key residues in the inhibitory mechanism of BPTI because it is one of the most

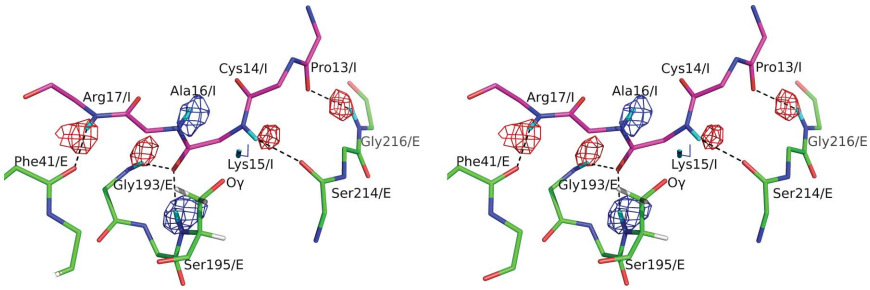

Figure 3
$F_o - F_c$ nuclear scattering maps (in stereoview) of the binding interface between the backbone of trypsin (in green) and the binding loop (P3 Arg17, P2 Ala16, P1 Lys15, P1′ Cys14 and P2′ Pro13) in BPTI (in magenta). The map was calculated without the inclusion of D and H atoms. The blue and red contours show $+3.0\sigma$ and -3.0σ levels, respectively. The broken lines indicate hydrogen bonds. This figure was prepared with *PyMOL*.

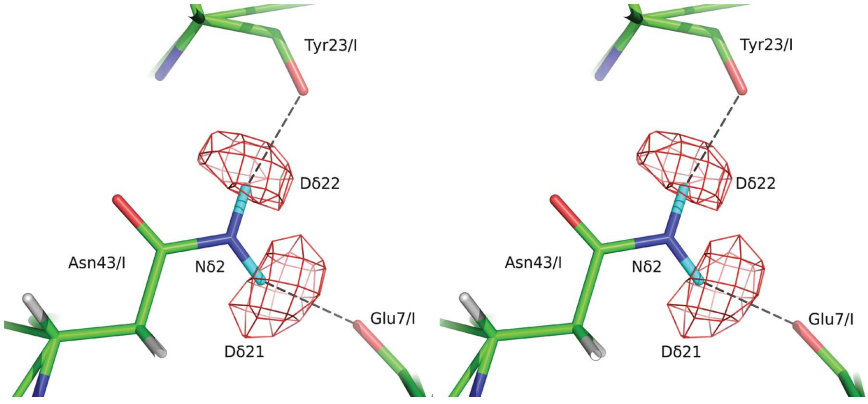

Figure 4
The $F_o - F_c$ nuclear-scattering map (in stereoview) of the Asn43 side chain, which was calculated upon omission of Asn43/I $D^{\delta21}$ and $D^{\delta22}$ and was prepared with *PyMOL*. The red contours show -3.0σ level density from hydrogen nuclei. The broken lines indicate the hydrogen bonds between the Asn43 side chain and the peptide O atoms of Glu7 and Tyr23 in BPTI.

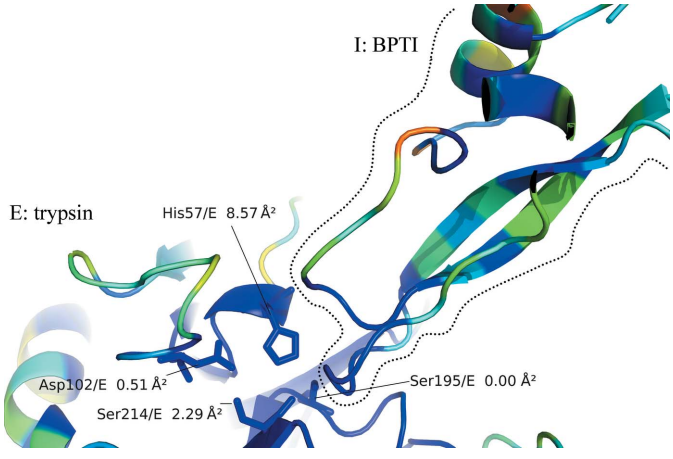

Figure 5
The accessible surface area (ASA) values around the active site in the trypsin–BPTI complex. The ASA values were calculated with *AREAIMOL* (Collaborative Computational Project, Number 4, 1994). The colour gradation from blue to red in the backbone of the ribbon model represents the range of ASA values from 0 to 211 Å^2, respectively. This figure was prepared with *PyMOL*.

highly conserved residues in BPTI homologues (Pritchard & Dufton, 1999; Dufton, 1985) and because the N43A mutant causes destabilization of the molecule (Bulaj & Goldenberg, 2001). The low H/D-exchange ratio of the NH_2 group in Asn43/E is attributed to the strong hydrogen bonds that make up the loop structure, which includes Tyr23/I and Glu7/I and contributes to rigidity. Collectively, this evidence suggests that Asn43/I is indeed one of the most important factors in the inhibitory mechanism of BPTI.

3.5. Why does irregular H/D exchange occur among residues in the local region?

As for other protein inhibitors, the commonly held hypothesis about how BPTI inhibits trypsin is that the former reacts rapidly with the latter to form a stable complex. It has been demonstrated that the associative strength of this complex is so high and that BPTI binds so tightly to trypsin (Vincent & Lazdunski, 1972) that hydrolytic water is unable to access the P1–P1′ reactive site and thus proteolysis is prevented (Laskowski & Wu, 1953; Blow *et al.*, 1972). According to this hypothesis, the main factor in inhibition is the inability of the hydrolytic water to approach the reactive site. In contrast, the essence of H/D exchange is that the heavy-water molecule approaches the reactive site to make the exchange. However, in this study we observed significant H/D exchange of both the amide H atom of the scissile peptide bond P1–P1′ and the H atom of the catalytic triad. The H/D-exchange ratios for His57 $D^{\delta1}$ and Ser195 D (D^{γ}) were both determined to be 100% and the ratio for the amide H atoms of Ala16/I was found to be 81% (Fig. 3).

One question that remains is how the H atoms of Ala16/I NH and H^{γ} between His57/E and Ser195/E were exchanged for D atoms. Furthermore, it is unclear why such irregular H/D exchanges occurred among residues in the local region. Regarding these issues, we propose the following hypothesis. The D_2O molecule approached the active site, although this was not observed using the X-ray or neutron diffraction methods. Of note, we evaluated the regions around His57/E–Asp102/E and Asp102/E–Ser214/E as possible gateways for the introduction of hydrolytic D_2O based on ASA calculations for these residues (Fig. 5). Subsequently, a solvent water molecule (D_2O, which acts as the catalyst for the H/D-exchange reaction) led to hydrolysis of the acyl bond when the acyl enzyme was formed (Finkenstadt & Laskowski, 1967; Blow *et al.*, 1972; Radisky & Koshland, 2002). Thus, D_2O made contact with the terminal Ala16 and the NH_2 of the cleaved

end of Ala16 became NHD or ND_2. Since the products remain part of the structure because of their tight binding to the enzyme, the reverse reaction for the reformation of a peptide bond between the Ala16 N-terminus and the Lys15 C-terminus occurred (Radisky & Koshland, 2002). As a result, the amide H atom of Ala16 was instead observed as a D atom. At the same time, the H atom (H^{γ}) of the hydroxyl group in Ser195 was exchanged for a D atom (D^{γ}) after receiving the D atom from the deuterated His57 $N^{\varepsilon 2}$. The cleaved segments of BPTI failed to leave their original positions because the interactions of the P1 Lys–S1 pocket and between P2′Arg17/I and Phe41/E were especially strong and the cleaved peptide was reformed by the reverse reaction, which is similar to the steps suggested previously by Zakharova *et al.* (2009).

4. Conclusions

In this study, we conducted the first neutron crystallographic analysis of the trypsin–BPTI complex and observed the protonation states of the active residues in the Michaelis complex of the serine protease. In this complexed state, a hydrogen bond between His57 and Ser195 increased the nucleophilic reactivity of the hydroxyl group of the serine.

In addition, we found that the different H/D-exchange ratios in the local region of the binding interface confirmed previous hypotheses and induced a new one which is detailed in the text. Our analyses confirmed that various contacts in the binding interface between BPTI and trypsin, including those between P2′ Arg17/I and Phe41/E, between P1 Lys15/I and Gly193/E, between P1 Lys15/I and Gly216/E and between P3Pro13/I and Ser214/E, form strong hydrogen bonds which bind the proteins tightly together. Our hypothesis is that the scissile peptide bond P1–P1′ of BPTI is hydrolyzed and the cleaved peptide is subsequently reformed by the catalytic reaction in the crystal phase.

The authors are grateful to Professors N. Igarashi and S. Wakatsuki of the Photon Factory (Proposal No. 2008G075) for X-ray data collection. The neutron experiment was performed under the Common-Use Facility Program of JAEA (2008A-A06). The work was mainly supported by the Ibaraki Prefectural Government and was supported in part by the Human Frontiers Science Program (Grant No. RGP0021/2006-C) and MEXT Grants-in-Aid for Scientific Research (Grant Nos. 20612002 and 21118502).

References

Adams, P. D., Mustyakimov, M., Afonine, P. V. & Langan, P. (2009). *Acta Cryst.* D**65**, 567–573.
Ardelt, W. & Laskowski, M. (1983). *Acta Biochim. Pol.* **30**, 115–126.
Ardelt, W. & Laskowski, M. (1985). *Biochemistry*, **24**, 5313–5320.
Blakeley, M. P. (2009). *Crystallogr. Rev.* **15**, 157–218.
Blakeley, M. P., Langan, P., Niimura, N. & Podjarny, A. (2008). *Curr. Opin. Struct. Biol.* **18**, 593–600.
Blow, D. M., Wright, C. S., Kukla, D., Rühlmann, A., Steigemann, W. & Huber, R. (1972). *J. Mol. Biol.* **69**, 137–144.
Bode, W. & Huber, R. (1992). *Eur. J. Biochem.* **204**, 433–451.
Bulaj, G. & Goldenberg, D. P. (2001). *J. Mol. Biol.* **313**, 639–656.
Collaborative Computational Project, Number 4 (1994). *Acta Cryst.* D**50**, 760–763.
Cotten, M., Fu, R. & Cross, T. A. (1999). *Biophys. J.* **76**, 1179–1189.
Deisenhofer, J. & Steigemann, W. (1975). *Acta Cryst.* B**31**, 238–250.
DeLano, W. L. (2002). *PyMOL.* http://www.pymol.org.
Dufton, M. J. (1985). *Eur. J. Biochem.* **153**, 647–654
Emsley, P. & Cowtan, K. (2004). *Acta Cryst.* D**60**, 2126–2132.
Englander, S. W., Sosnick, T. R., Englander, J. J. & Mayne, L. (1996). *Curr. Opin. Struct. Biol.* **6**, 18–23.
Fasoli, E., Ferrer, A. & Barletta, G. L. (2009). *Biotechnol. Bioeng.* **102**, 1025–1032.
Finkenstadt, W. R. & Laskowski, M. (1967). *J. Biol. Chem.* **242**, 771–773.
Fisher, S. J. & Helliwell, J. R. (2008). *Acta Cryst.* A**64**, 359–367.
Fritz, H. & Wunderer, G. (1983). *Arzneimittelforschung*, **33**, 479–494.
Garcia, R. A., Pantazatos, D. & Villarreal, F. J. (2004). *Assay Drug Dev. Technol.* **2**, 81–91.
Greene, L. J., Rigbi, M. & Fackre, D. S. (1966). *J. Biol. Chem.* **241**, 5610–5618.
Hamuro, Y., Coales, S. J., Southern, M. R., Nemeth-Cawley, J. F., Stranz, D. D. & Griffin, P. R. (2003). *J. Biomol. Tech.* **14**, 171–182.
Hanson, W. M., Domek, G. J., Horvath, M. P. & Goldenberg, D. P. (2007). *J. Mol. Biol.* **366**, 230–243.
Hedstrom, L. (2002). *Chem. Rev.* **102**, 4501–4524.
Huber, R. & Bode, W. (1978). *Acc. Chem. Res.* **11**, 114–122.
Huber, R., Kukla, D., Bode, W., Schwager, P., Bartels, K., Deisenhofer, J. & Steigemann, W. (1974). *J. Mol. Biol.* **89**, 73–101.
Huber, R., Kukla, D., Rühlmann, A., Epp, O. & Formanek, H. (1970). *Naturwissenschaften*, **57**, 389–392.
Iwai, W., Yamada, T., Kurihara, K., Ohnishi, Y., Kobayashi, Y., Tanaka, I., Takahashi, H., Kuroki, R., Tamada, T. & Niimura, N. (2009). *Acta Cryst.* D**65**, 1042–1050.
Kaltashov, I. A., Bobst, C. E. & Abzalimov, R. R. (2009). *Anal. Chem.* **81**, 7892–7899.
Kossiakoff, A. A. (1984). *Basic Life Sci.* **27**, 281–304.
Krowarsch, D., Zakrzewska, M., Smalas, A. O. & Otlewski, J. (2005). *Protein Pept. Lett.* **12**, 403–407.
Kurihara, K., Tanaka, I., Refai Muslih, M., Ostermann, A. & Niimura, N. (2004). *J. Synchrotron Rad.* **11**, 68–71.
Laskowski, M. & Qasim, M. A. (2000). *Biochim. Biophys. Acta*, **1477**, 324–337.
Laskowski, M. Jr & Sealock, R. W. (1971). *The Enzymes*, Vol. 3, edited by P. D. Boyer, pp. 375–473. New York: Academic Press.
Laskowski, M. & Wu, F. C. (1953). *J. Biol. Chem.* **204**, 797–805.
Li, Z., Wan, H., Shi, Y. & Ouyang, P. (2004). *J. Chem. Inf. Comput. Sci.* **44**, 1886–1890.
Liu, W. H., Means, G. E. & Feeney, R. E. (1971). *Biochim. Biophys. Acta*, **229**, 176–185.
Marquart, M., Walter, J., Deisenhofer, J., Bode, W. & Huber, R. (1983). *Acta Cryst.* B**39**, 480–490.
Niimura, N. & Bau, R. (2008). *Acta Cryst.* A**64**, 12–22.
Otlewski, J., Jaskólski, M., Buczek, O., Cierpicki, T., Czapińska, H., Krowarsch, D., Smalas, A. O., Stachowiak, D., Szpineta, A. & Dadlez, M. (2001). *Acta Biochim. Pol.* **48**, 419–428.
Otlewski, J., Jelen, F., Zakrzewska, M. & Oleksy, A. (2005). *EMBO J.* **24**, 1303–1310.
Otwinowski, Z. & Minor, W. (1997). *Methods Enzymol.* **276**, 307–326.
Pritchard, L. & Dufton, M. J. (1999). *J. Mol. Biol.* **285**, 1589–1607.
Radisky, E. S. & Koshland, D. E. (2002). *Proc. Natl Acad. Sci. USA*, **99**, 10316–10321.
Rühlmann, A., Kukla, D., Schwager, P., Bartels, K. & Huber, R. (1973). *J. Mol. Biol.* **77**, 417–436.
Schechter, I. & Berger, A. (1967). *Biochem. Biophys. Res. Commun.* **27**, 157–162.
Simon, I., Tuchsen, E. & Woodward, C. (1984). *Biochemistry*, **23**, 2064–2068.

Tamada, T., Kinoshita, T., Kurihara, K., Adachi, M., Ohhara, T., Imai, K., Kuroki, R. & Tada, T. (2009). *J. Am. Chem. Soc.* **131**, 11033–11040.
Vincent, J. P. & Lazdunski, M. (1972). *Biochemistry*, **11**, 2967–2977.
Voet, D., Voet, J. G. & Pratt, C. W. (1999). *Fundamentals of Biochemistry*. New York: John Wiley & Sons.
Wagner, G. & Wüthrich, K. (1982). *J. Mol. Biol.* **160**, 343–361.
Wales, T. E. & Engen, J. R. (2006). *Mass Spectrom. Rev.* **25**, 158–170.
Wlodawer, A., Nachman, J., Gilliland, G. L., Gallagher, W. & Woodward, C. (1987). *J. Mol. Biol.* **198**, 469–480.
Wlodawer, A., Walter, J., Huber, R. & Sjölin, L. (1984). *J. Mol. Biol.* **180**, 301–329.
Yagi, D., Yamada, T., Kurihara, K., Ohnishi, Y., Yamashita, M., Tamada, T., Tanaka, I., Kuroki, R. & Niimura, N. (2009). *Acta Cryst.* D**65**, 892–899.
Zakharova, E., Horvath, M. P. & Goldenberg, D. P. (2009). *Proc. Natl Acad. Sci. USA*, **106**, 11034–11039.